Ecological Indicators 126 (2021) 107707

Contents lists available at ScienceDirect

Ecological Indicators

journal homepage: www.elsevier.com/locate/ecolind

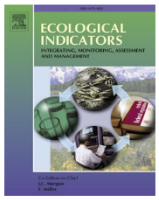

# Urban trees for biomonitoring atmospheric particulate matter: An integrated approach combining plant functional traits, magnetic and chemical properties

Lina Fusaro [a,b,*], Elisabetta Salvatori [c], Aldo Winkler [d], Maria Agostina Frezzini [b], Elena De Santis [b], Leonardo Sagnotti [d], Silvia Canepari [b], Fausto Manes [b]

[a] National Research Council, Institute of BioEconomy, Via dei Taurini 19, 00185 Rome, Italy
[b] Department of Environmental Biology, Sapienza University of Rome, p.le Aldo Moro 5, 00185 Rome, Italy
[c] ENEA, Italian National Agency for New Technologies, Energy and Sustainable Economic Development, SSPT – STS, R.C. Casaccia, Via Anguillarese, 301, 00123 S. Maria di Galeria, Rome, Italy
[d] Istituto Nazionale di Geofisica e Vulcanologia, Via di Vigna Murata 605, 00143 Rome, Italy

ARTICLE INFO

*Keywords:*
PM injury
Biomonitoring
Urban green
Functional traits
Magnetic properties
Oxidative potential

ABSTRACT

Increased attention has been given to particulate matter (PM) that, as well as worsening air quality, is responsible for chronic and acute respiratory or cardiovascular diseases. Currently, most of the studies are focused on the capacity of plants and other biological media to adsorb PM, whereas few works explore the functional damage due to PM on urban vegetation. The present study, considering *Quercus ilex* L. as target species for its wide distribution in the Mediterranean urban and natural areas, pointed out that PM accumulation, inferred from magnetic and chemical properties, has almost no effects on structural morpho-functional traits as Relative Water Content or Specific Leaf Area but can impair processes related to the first photochemical reactions suggesting shading effect on leaves. PSI functionality and thus, carbon assimilation related processes, are impaired to a lesser extent by the oxidative potential of PM. Our results showed that, although several oxidative stressors can simultaneously affect morpho-functional traits, the interdisciplinary approach tested here can be a key tool to enlarge the spatial scale of biomonitoring activities as much as possible, and highlight a functional indicator of PM injury. This is needed to enhance the knowledge about the complex processes that are implied in the dynamic relationship between air quality, vegetation functionality and ecosystem services provisioning in urban areas.

## 1. Introduction

Nowadays, air pollution is a major concern especially in the urban environment, where most of the global population lives. Emission of atmospheric pollutants is strictly connected with human activities, industries and, above all, combustion processes, which produce a large number of pollutants, whose chemical composition is extremely heterogeneous (WHO, 2004). Among them, particulate matter (PM), a complex mixture of solid particles and liquid droplets of different diameters and chemical nature, is one of the most dangerous and harmful pollutants for human health (Costabile et al., 2020).

Indeed, it is well known that PM pollution causes stroke, chronic and acute respiratory or cardiovascular diseases (Orioli et al., 2019), and it is linked to premature mortality. It was estimated that in 2016 indoor and outdoor air pollution caused 7 million deaths worldwide, that are mainly due to the exposure to fine and ultrafine PM of 2.5 μm or less in diameter ($PM_{2.5}$) (WHO, 2014). Furthermore, recent studies have hypothesized a positive association between the concentration of airborne $PM_{10\text{-}2.5}$ and the spread of the novel Coronavirus (SARS-CoV-2), (Comunian et al., 2020; Setti et al., 2020; Yao et al., 2020; Zoran et al., 2020). In particular, it has been suggested that high PM pollution can either trigger lung inflammation and enhance the population sensitivity to the virus (Conticini et al., 2020; Fattorini and Regoli, 2020), or act as a direct virus "carrier", thus increasing the risk of its airborne diffusion (di Toppi et al., 2020; Tung et al., 2021).

In urban areas, trees and shrubs play an important role in removing air pollutants, especially particulate ones, through dry deposition on the leaf surface (Blanusa et al., 2015). Plants improve air quality providing

* Corresponding author at: National Research Council, Institute of BioEconomy, Via dei Taurini 19, 00185 Rome, Italy.
*E-mail address:* lina.fusaro@cnr.it (L. Fusaro).

https://doi.org/10.1016/j.ecolind.2021.107707
Received 26 December 2020; Received in revised form 7 April 2021; Accepted 8 April 2021
Available online 17 April 2021

an important ecosystem service to the population serving as a natural sink for pollutants (Fusaro et al., 2017a; Manes et al., 2016; Mukherjee and Agrawal, 2018). Since the greater the tree cover, the greater the pollution removal, urban vegetation can be used for phytoremediation, but also air monitoring: plants can be used as biomonitors through ecological investigation thanks to their simple identification and sampling, their ubiquity and their large amount of biomass (Nowak et al., 2006). On the other side, PM can damage plants that are the primary receptors for air pollutants (Stevens et al., 2020).

In this context, leaf functional traits (FT), i.e. morphological, physiological and phenological characteristics that influence plant performance and its function in the ecosystem (Violle et al., 2007), can play a pivotal role in both phytoremediation and biomonitoring. FT influence the ecological efficiency of plant species in removing PM, since it depends on leaf shape and morphological features (Grote et al., 2016; Sæbø et al., 2012), and are useful for screening plant health, used as indicators of air pollution and other environmental stress injuries (Bussotti and Pollastrini, 2015).

Rai (2016) made an exhaustive overview of the reached results on the physiological, biochemical and morphological alterations caused by PM, showing that PM deposition on leaves negatively affects photosynthetic activity and protein synthesis, also increasing plant susceptibility to pathogens.

PM can have remarkable magnetic properties arising from magnetite-like ferrimagnetic particles (Flanders, 1994; Hunt et al., 1984), often associated with heavy metals such as Cd, Cr, Zn (Georgeaud et al., 1997; Hunt et al., 1984). The magnetic properties of PM may arise from combustion processes related to industry, domestic heating, or vehicles, as well as from abrasion products from street surfaces and brake systems (e.g. Hoffmann et al., 1999; Jordanova et al., 2004). Especially in urban areas, vehicular traffic represents the main source of PM associated with magnetite-like minerals (Gonet and Maher, 2019; Sagnotti et al., 2009), mostly emitted by the abrasion of disk brakes (Chaparro et al., 2020; Gonet et al., 2021; Winkler et al., 2020). In urban contexts, the magnetic susceptibility of leaves decreases with increasing distance from the roadside, confirming the relationship between vehicular traffic and the emission of magnetic iron (Szönyi et al., 2007).

Rock magnetism methods have been widely used to biomonitoring air pollution using tree leaves, barks, mosses and lichens, being efficient PM receptors (for a review, Hofman et al., 2017). Magnetic properties detected on tree leaves mostly depend on the concentration and the grain size of magnetite-like minerals accumulated on the samples, with the magnetic susceptibility being the fastest, most used and practical parameter (Kapper et al., 2020).

To better understand the biological responses to PM of living organisms, the oxidative potential (OP) of particles can be assessed. OP provides a proxy of the oxidative capacity of PM and the oxidative stress processes, hypothesizing that PM components cause the formation of reactive oxygen species (ROS), that can lead to the membrane and cell damages (Ficociello et al., 2020; Piacentini et al., 2019; Simonetti et al., 2018). Among existing OP acellular assays, the ascorbic acid ($OP^{AA}$), which is expressed as the consumption rate of AA by particles over time, has been widely assessed as an indicator of particles OP (Campbell et al., 2019; Pietrogrande et al., 2019). $OP^{AA}$ measurement seems to be particularly influenced by inorganic components and, in detail, different studies support that non-exhaust traffic emissions affect $OP^{AA}$ results (Bates et al., 2019; Massimi et al., 2020). Indeed, ascorbic acid is a physiological, non-enzymatic antioxidant located in the apoplast and used as a defense against ROS; it increases under high pollution conditions, being one of the most sensitive leaf functional traits to air pollutants (Mukherjee and Agrawal, 2018).

Ecophysiological, magnetic and chemical methods are all useful tools to determine PM harmful effects on urban vegetation as well as the composition of particulate matter and the grain size, assuming a significant role in biomonitoring air pollution. Although the importance of such methods is widely known, still very few works have focused on the correlation between these three scientific fields, showing a lack of interdisciplinary studies related to PM. In this context, an integrated approach is crucial to achieving a better comprehension of the effects of PM and the biological response it induces on urban vegetation. In this paper, we measured leaf functional traits, like the specific leaf area (SLA), the relative content of chlorophyll and the chlorophyll *a* fluorescence, correlating them with both magnetic properties and oxidative potential of PM deposited on leaves, determining also the elemental composition of the bioaccumulated particles. *Quercus ilex* L. has been chosen as target species for its widespread use in urban contexts in the Mediterranean urban areas and for its efficiency in accumulating magnetic PM (Moreno et al., 2003). The hypothesis to be tested is that the photosynthetic performance of *Q. ilex* decreases with increasing values of magnetic susceptibility, which is considered a proxy of the accumulation of traffic-related magnetic dust.

The experimental field campaign tests if the applied integrative approach can be used as an effective tool to biomonitoring air quality and the vegetation stress condition related to PM exposure and accumulation. Since PM can affect photosynthesis through several physiological mechanisms from impairing photosystems functionality, slowing down the processes related to the first photochemical reactions, to affecting the reduction of end acceptors on PSI side, or damaging the pigments, it could be highly valuable to finalize the analysis of strengths and weakness of biomonitoring to highlight the most suitable functional indicators.

## 2. Material and methods

### 2.1. Sites selection and characterization

The sampling was conducted within the city of Rome, Italy, in sites where *Q. ilex* trees were present, having comparable age and morphological characteristics (diameter at breast height between 0.80 and 1.20 m, crown radius ranging from 1 to 2 m) and for which the outer part of the crown was accessible.

In particular, eight sites were selected (Fig. 1): Castelporziano Estate (CP), Villa Ada urban park (VA), Porta Pinciana (PP), Via Salaria (VS), Viale Mazzini (MZ), Quirino Majorana (QM), Re di Roma (RdR), Vigna Murata (VM). The sites selection was based on the following criteria i) the characteristics of the green infrastructure element (Bolund and Hunhammar, 1999): peri-urban forest, CP; urban forest, VA; street tree lines, PP, VS, MZ, QM; trees in an open square, RdR; grouped trees in large lawn, VM; ii) the site's location in respect to the city centre, and in different urban settlements; iii) the annual average $PM_{10}$ concentrations ($\mu g\ m^{-3}$) derived, for each experimental site, from integrated modelling system (Sebastiani et al., 2021) (Table 1).

Furthermore, seasonal $PM_{10}$ concentration (recorded from Regional Environmental Protection Agency, ARPA Lazio, monitoring network) of the urban settlements considered in the present study, was also taken into account, for an indication of the mean state of the air quality, considering only those monitoring stations located nearby the experimental sites (Appendix A and B).

Specifically, CP is a natural peri-urban forest within a protected area of about 6000 ha, located 25 km from Rome city centre and close to the Tyrrhenian coast (3 km) (Fig. 1). Annual $PM_{10}$ concentration in this site is the lowest (12 $\mu g\ m^{-3}$, Table 1). VA site is instead a fairly well preserved natural forest (Fusaro et al., 2019a, 2019b) located inside the urban forest of a historical Villa that, with an extension of 160 ha, is one of the largest urban parks in the Rome city centre (Fig. 1). VA has a higher annual concentration of $PM_{10}$ than CP (22 $\mu g\ m^{-3}$), but lower than the other sites (Table 1), comparable to the urban background level (Canepari et al., 2009, Appendix A). Based on the green infrastructure characteristics (natural forests) as well as on the PM annual values, not directly affected by traffic-related emissions, CP and VA were considered as control sites. In PP site, the sampled trees are street trees close to a traffic light, located at the borders of the large urban park of Villa

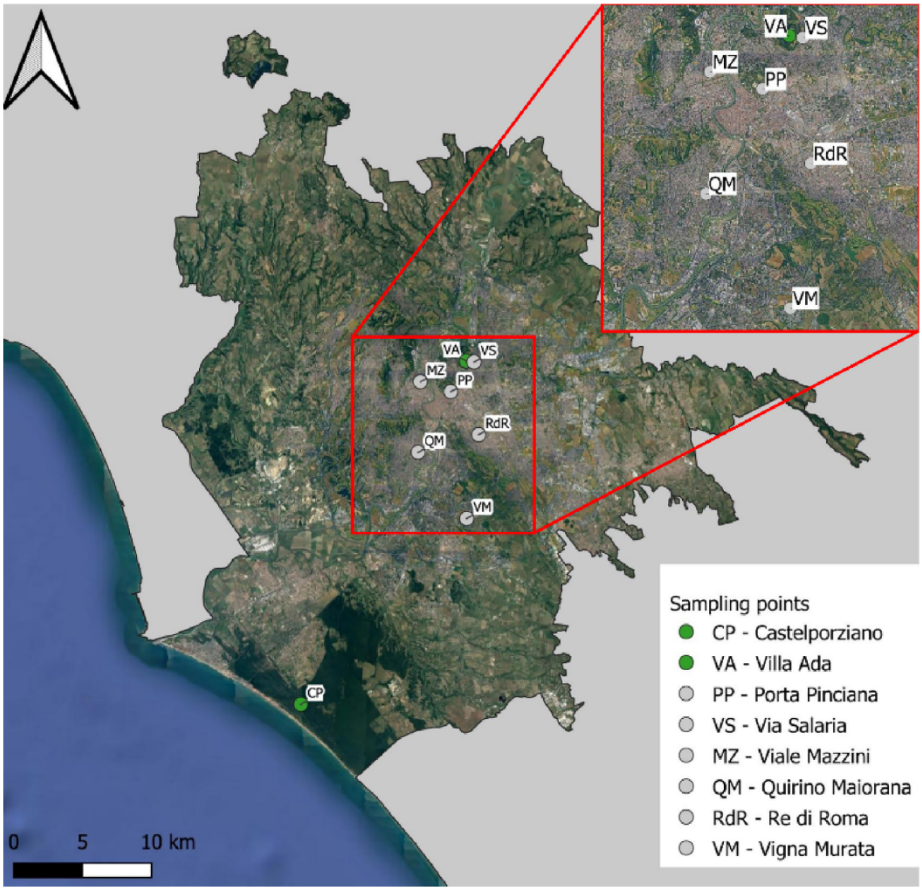


**Fig. 1.** Spatial distribution of experimental sites. The green markers represent the control sites of Castelporziano Estate (CP) and Villa Ada urban park (VA) (see text for further details). (For interpretation of the references to colour in this figure legend, the reader is referred to the web version of this article.)

**Table 1**
$PM_{10}$ annual mean concentration (μg $m^{-3}$) for each experimental site was retrieved from the integrated modeling system elaborated by Regional Environmental Protection Agency monitoring network, ARPA Lazio, 2018 (Sebastiani et al., 2021).

| Experimental site | $PM_{10}$ annual mean |
|---|---|
| CP | 12 |
| VA | 22 |
| MZ | 23 |
| PP | 25 |
| VM | 25 |
| RdR | 26 |
| VS | 26 |
| QM | 27 |

Borghese, in the historical city centre. $PM_{10}$ average annual concentration in this site is 25 μg $m^{-3}$ (Table 1). VS, MZ and QM are all street trees with similar green infrastructure characteristics (linear elements, surrounded by impervious surfaces) but are located in different urban contexts.

In particular, VS site is in the city centre, close to VA (Fig. 1), and borders an intense traffic road, traveled by more than 2000 vehicles per hour (Rome Municipality, 2020; Alessio et al., 2002), is therefore characterized by high annual $PM_{10}$ levels (26 μg $m^{-3}$, Table 1). MZ is placed in a residential neighborhood in the city centre, with better air quality ($PM_{10}$ = 23 μg $m^{-3}$, Table 1), while QM is located in a densely urbanized neighborhood in the South-Western part of the city, close to via Portuense avenue, with a high traffic rate (2050 vehicles/h, Rome Municipality, 2020) and the highest $PM_{10}$ annual values (27 μg $m^{-3}$, Table 1).

RdR site is in a large circular open square lined by *Q. ilex* trees, located in the commercial area in the central-southern part of the city (Fig. 1), characterized by intense car traffic (2200 vehicles/h, Rome Municipality, 2020) and, accordingly, fairly high PM concentration (annual mean 26 μg $m^{-3}$, Table 1). Finally, in VM site, the sampled trees are grouped in a lawn along an expressway in a suburban area of the south-western quadrant of the city, characterized by a lower urbanization density and by the presence of large agricultural and semi-natural spaces (Fig. 1). VM has an average annual $PM_{10}$ concentration of 23 μg $m^{-3}$ (Table 1) and is close to via Laurentina, an avenue traveled by around 1500 vehicles/h (Municipality of Rome, 2020).

### 2.2. Experimental design

The field campaign was carried out on 6 and 7 March 2019 during two consecutive days with stable meteorological conditions, more than 15 days from the last rain event, to avoid the influence of rainfall on the PM leaf deposition (Xu et al., 2017). Indeed, the last rain event registered by the Servizio Integrato Agrometeorologico della Regione Lazio in the Rome city centre (Lanciani Station, 41° 92′ N, 12°52′ E) was registered on February 11th. In March the minimum temperature was 8.10 ± 1.77, maximum was around 18.13 ± 2.52 and the mean was 12.81 ± 1.40, with four rainy days after the 12 of March.

For each experimental site, four to five representative adult trees were sampled, and sun-exposed, fully developed leaves, were collected at 1.50 m height from the outer part of the crown next to the road. For each tree, twigs were detached, stored in sealed plastic bags to avoid dehydration, and brought to the laboratories where morpho-functional traits, magnetic properties and chemical analysis were carried out. In

particular, for each tree, twigs were collected in three different portions of the crown to represent the natural variability of light and PM exposure in the crown of the urban street trees (Janhäll, 2015; Sgrigna et al., 2015). In each crown portion, 3 twigs were sampled: one was used for morpho-functional traits measurements, one for magnetic and one for chemical analysis. Morpho-functional traits were measured on one leaf for each twig and data were aggregated for each sampled tree (n = 4–5). For magnetic and chemical analysis, leaves collected from the twigs were pulled together and measurements were performed on three subsamples for each site (n = 3).

### 2.3. Magnetic characterization

Magnetic measurements were performed at the paleomagnetic laboratory of INGV. Dried leaves were pressed inside 8 $cm^3$ plastic cubes for measuring the mass-specific magnetic susceptibility ($\chi$), which was determined on AGICO KLY5 Kappabridge dividing the bulk susceptibility values, after subtraction of the empty holder, for the net weight of the samples.

Leaves fragments, irregularly dimensioned and shaped, were pushed inside pharmaceutical gel caps #4, around 0.15 mL capacity, for the hysteresis characterization with the Princeton Measurement Corporation Micromag 3900 Vibrating Sample Magnetometer (VSM).

The coercive force ($B_C$), the saturation remanent magnetization ($M_{RS}$, or SIRM) and the saturation magnetization ($M_S$) were measured in magnetic fields up to 1.0 T and their values were calculated after subtracting the high field linear paramagnetic trend, achieved after saturation of the ferromagnetic component. Mass-specific magnetization values for the concentration-dependent magnetic parameters were calculated dividing the magnetic moments by the net weight of the samples. The coercivity of remanence ($B_{CR}$) was extrapolated from backfield remagnetization curves up to −1 T, following forward magnetization in a +1 T field. The magnetic measurements were performed on dried leaves since the content of water influences the mass and the susceptibility of the samples (Szönyi et al., 2008).

Moreover, the domain state and magnetic grain-size of the magnetic particles of the samples were compared to theoretical magnetite according to the hysteresis ratios $M_{RS}$ /$M_S$ vs. $B_{CR}$ /$B_C$ in the "Day plot" (Day et al., 1977; Dunlop, 2002a, 2002b).

### 2.4. Morpho-functional traits measurements

Leaf- Relative Water Content (RWC, %) was calculated as follows:

$$\mathrm{RWC} = \frac{FW - DW}{TW - DW} \times 100$$

where FM is leaf fresh mass, DW is leaf dry mass, and TW is leaf turgor mass, water-saturated leaf weight measured after 10–12 h in water saturating conditions (petiole in water). Then leaves were dried in the oven at 80 °C until the stable dry weight was reached. Specific Leaf Area ($cm^2$ $gr^{-1}$) was measured on the same leaves collected for RWC, calculated as the ratio between leaf area and dry weight.

The relative chlorophyll content, $Chl_{SPAD,}$ was estimated in vivo using a portable chlorophyll meter (SPAD-502DL Plus, 160 Minolta; Spectrum Technologies Ltd., Plainfield, IL, USA). This instrument provides an estimation of the relative amount of leaf chlorophyll content based on the transmitted radiation in the red and near-infrared wavelengths and the resulting values are reported in arbitrary units.

Chlorophyll *a* fluorescence, ChlF, measurements were performed after 1 h of sample dark adaptation, necessary to reduce the effects of transient photoinhibition (Desotgiu et al., 2012).

After dark adaptation, the primary acceptors reach a complete oxidation state and then are exposed to a saturating red actinic light pulse of 3000 μmol photons $m^{-2}$ $s^{-1}$ of 1 s duration and the kinetics of the polyphasic prompt fluorescence transient (FT) rise is recorded by a direct fluorometer, Handy PEA (Hansatech Instruments, Norfolk, UK). The FT plotted on a logarithmic time-scale, exhibits a series of steps labeled as O ($F_0$, when all the reaction centres of the PSII are open) J (2 ms), I (30 ms) and maximum P level (Fm, when all the PSII reaction centres are fully reduced). The first part of the FT (O–J) expresses the photochemical events, giving information about the accumulation of reduced QA (primary electron acceptor quinone of PSII). The J–I–P region of the FT reflects the velocity of ferredoxin reduction beyond the PSI. The FT was elaborated using the JIP-test, a tool that translates this polyphasic fluorescence transient into a constellation of biophysical parameters, which quantify the single steps of the photochemical pathway through both photosystem II (PSII) and photosystem I (PSI) (Strasser et al., 2010). In this study the following JIP-test parameters were considered: RC/ABS, a pool of active reaction centre (RC) per PSII antenna complex; $DI_0$/RC, effective dissipation in an active RC; $TR_0$/RC, reducing QA energy flow for each RC; $ET_0$/RC, the electron transport beyond $QA^-$ per RC; $\Delta V_{IP}$, the efficiency of electron transport to reduce the end acceptors beyond the PSI; $PI_{TOT}$, Total Performance Index (potential) for energy conservation from photons absorbed by PSII to the reduction of PSI end acceptors.

### 2.5. Chemical characterization

For each sites, three replicates of 10 leaves randomly chosen as subsample, were put in the Falcon tubes with 50 mL of deionized water (produced by Arioso UP 900 Integrate Water Purification System, USA) and, then, stirred for 30 min with a rotary shaker (60 rpm; Rotator; GlasCol, USA) to extract the water-soluble fraction of PM deposited on leaves. After the extraction, the solutions were filtered through a cellulose nitrate filter (0.45 μm pore size, Merck Millipore Ltd., Billerica, MA, USA). Consequently, the solutions were split into proper aliquots to perform AA assay and chemical analyses through the utilization of inductively coupled plasma mass spectrometry (ICP-MS, Bruker 820-MS, Billerica, MA, USA).

AA assay was performed on water-soluble fraction of samples, following previously detailed and widely used procedures (Frezzini et al., 2019; Massimi et al., 2020). Briefly, 2.5 mL of the filtered aqueous extracts were mixed with 300 μL of phosphate buffer (0.5 mM at pH 7.4) and 100 μL of ascorbic acid solution (2 mM). Then, the depletion of AA was monitored for 20 min by recording the decrease in absorbance by UV–Vis spectroscopy at 265 nm (Varian Cary 50 Bio UV–Vis; Varian Inc., Palo Alto, CA, USA). $OP^{AA}$ was calculated as the depletion rate per unit of mass of sampled leaves (nmol AA $min^{-1}$ $g^{-1}$) using the following equations:

$$o'AA = -o'Abs \times \frac{N_0}{Abs_0}, \quad OP^{AA} = \frac{o'AA_s - o'AA_b}{\frac{V_a}{V_e} \times V_S}$$

where σAbs is the slope of the absorbance of blanks vs. time (min-1), $Abs_0$ is the initial absorbance calculated from the intercept of the linear regression between absorbance and. time, $N_0$ is the number of AA moles added for the reaction (200 nmol), σAAs and σAAb are the rate of AA consumption for the sample and the blank, respectively (nmol $min^{-1}$), $V_e$ and $V_a$ are the extraction volume (50 mL) and sample volume added to the reaction vial (2.5 mL) respectively, and m is the leaves dry weights of each leaves sample (g).

The concentrations (ng $g^{-1}$) of 29 inorganic elements (Al, As, B, Ba, Be, Cd, Ce, Co, Cr, Cs, Cu, Fe, K, La, Mn, Mo, Ni, Pb, Rb, Sb, Se, Sn, Sr, Ti, Tl, V, W, Zn and Zr) were determined in water-extracted fractions by adapting an analytical procedure allowing the determination of PM micro-components and trace elements (Canepari et al., 2006).

### 2.6. Statistical analysis

All data i.e. seasonal PM air concentration, magnetic measurements, morpho-functional traits, chemical analysis were compared using one-

way ANOVA with the site as a fixed factor, and the means significantly different at $p < 0.05$ were identified using post hoc Student–Neuman–Keuls test. A multivariate statistical technique, the Principal Component Analysis (PCA), was used to investigate the structures of variability within the different experimental sites. The selection of the principal factors was based on those with eigenvalues greater than 1.

Pearson correlation analysis was performed to assess the applicability of morpho-functional traits as indicators of PM damage, testing the relationship between traits (RWC, SLA, $Chl_{SPAD}$, JIP-test parameters) magnetic measurements and chemical analysis. Data were aggregated at the site level. All analyses were performed using Statistica software, version 7.0 (StatSoft, Tulsa OK, USA).

## 3. Results

### 3.1. Magnetic properties

Mass specific magnetic susceptibility values, at the site level, ranged from 0.9 to 44.6 $\times 10^{-8}$ $m^3$ $kg^{-1}$ (Fig. 2), and the lowest values were measured in the CP samples. Low values were measured also in VA (the urban forest inside a large green park) and MZ (street trees in a residential neighborhood). PP, VM had an intermediate susceptibility whereas RdR, VS and QM showed the highest susceptibility.

The hysteresis loops measured on all samples were similar in shape: narrow, saturated well before 1 T (Appendix C), with a modest variability of both coercivities (5.9 mT < $B_C$ < 7.7 mT; 34.0 mT < $B_{CR}$ < 41.6 mT, at site level). All the samples from site CP and one sample from VA, whose magnetization was too low to produce hysteresis loops satisfactory defined, were neglected.

The concentration-dependent magnetic parameters obtained from hysteresis loops varied, at the site level, from 1.6 to 32.7 $mAm^2kg^{-1}$ and from 0.1 to 2.3 $mAm^2kg^{-1}$ for $M_S$ and $M_{RS}$, respectively, and SIRM/ $\chi$ values, at the site level, ranged from 3.38 to 6.21 kA/m.

It was not possible to estimate the Curie temperature using magnetothermic cycles, due to the low susceptibility values and the disturbance caused by the burning of organic matter during heating.

The $M_{RS}/M_S$ vs. $B_{CR}/B_C$ ratios (Fig. 3) show that the values from all sites are located in a cluster in the middle-right side of the Day plot, between the theoretical curves calculated for mixtures of a single domain (SD) and multidomain (MD) magnetite grains and for a mixture of SD and superparamagnetic (SP) magnetite grains (Dunlop, 2002a, 2002b).

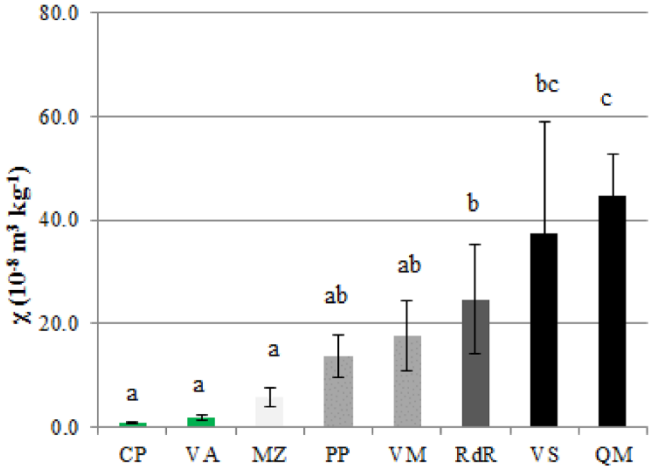


**Fig. 2.** Magnetic susceptibility of *Q. ilex* leaves in the different experimental sites. Bars denote mean ± standard deviation, and those not accompanied by the same letters are significantly different at $p < 0.05$.

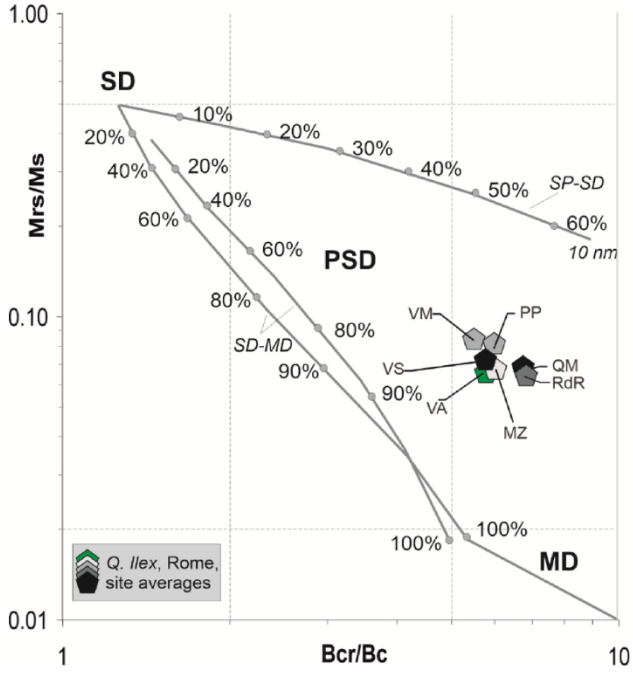


**Fig. 3.** Bilogarithmic Day plot of the hysteresis ratios $M_{RS}/M_S$ vs. $B_{CR}/B_C$. Data are shown as site averaged; pentagons' colours according to the site classification. SD: single domain; PSD: pseudo single domain; MD: multi domain; SP: superparamagnetic.

### 3.2. Morpho-functional traits

All sites presented close values of RWC, except for PP that showed the minimum value and MZ the maximum. SLA was slightly but significantly lower in control sites CP and VA, as well as in VM, meaning higher sclerophyll degree. MZ presented high SLA, i.e. the lowest sclerophyll degree, together with the sites with high PM accumulation (RdR, VS, QM). The lowest $Chl_{SPAD}$ values were measured in CP and VS, the highest in VA. No substantial differences were detected among the other experimental sites (Table 2).

The values of JIP-test parameters are shown in Fig. 4 in the different sites. RC/ABS had lower values in the sites characterized by the higher susceptibility (RdR, VS, QM), increasing in intermediate and control sites (Fig. 4 a). The dissipation per active reaction centre ($DI_0$/RC, Fig. 4 b) followed an opposite pattern: the lowest values were measured in the VA, MZ, CP and VM sites. $DI_0$/RC slightly increased going towards the sites with higher magnetic susceptibility values (RdR, and VS) with the exceptions of QM that presented $DI_0$/RC comparable to the control sites CP, and with those presented an intermediate accumulation as PP.

The functional parameters which expressed the specific energy fluxes (per QA reducing PSII RC), as $TR_0$/RC and $ET_0$/RC, increased in the sites

**Table 2**
Relative Water Content (%), Specific Leaf Area ($cm^2$ $gr^{-1}$) and Chlorophyll relative content, $Chl_{SPAD}$ (SPAD units) measured in the experimental sites. Values express mean ± standard deviation and those not accompanied by the same letters are significantly different at $p < 0.05$. n, indicates the number of replicates for each site (sampled trees).

| Site | RWC | SLA | $Chl_{SPAD}$ | n |
|---|---|---|---|---|
| CP | 81.90 ± 4.44ab | 64.16 ± 10.38a | 47.37 ± 1.72a | 4 |
| VA | 80.45 ± 8.82ab | 61.82 ± 1.24a | 54.04 ± 2.84b | 5 |
| MZ | 90.88 ± 7.35b | 85.11 ± 11.8b | 51.66 ± 2.53ab | 4 |
| PP | 67.15 ± 16.6a | 75.82 ± 4.12ab | 52.13 ± 4.65ab | 4 |
| VM | 81.22 ± 4.6ab | 64.07 ± 6.5a | 51.52 ± 3.35ab | 5 |
| RdR | 79.95 ± 10.7ab | 82.20 ± 12.3b | 49.7 ± 1.85ab | 5 |
| VS | 81.73 ± 3.22ab | 86.09 ± 7.8b | 48.70 ± 4.48ab | 5 |
| QM | 77.16 ± 10.08ab | 77.52 ± 7.9ab | 50.75 ± 2.51ab | 5 |

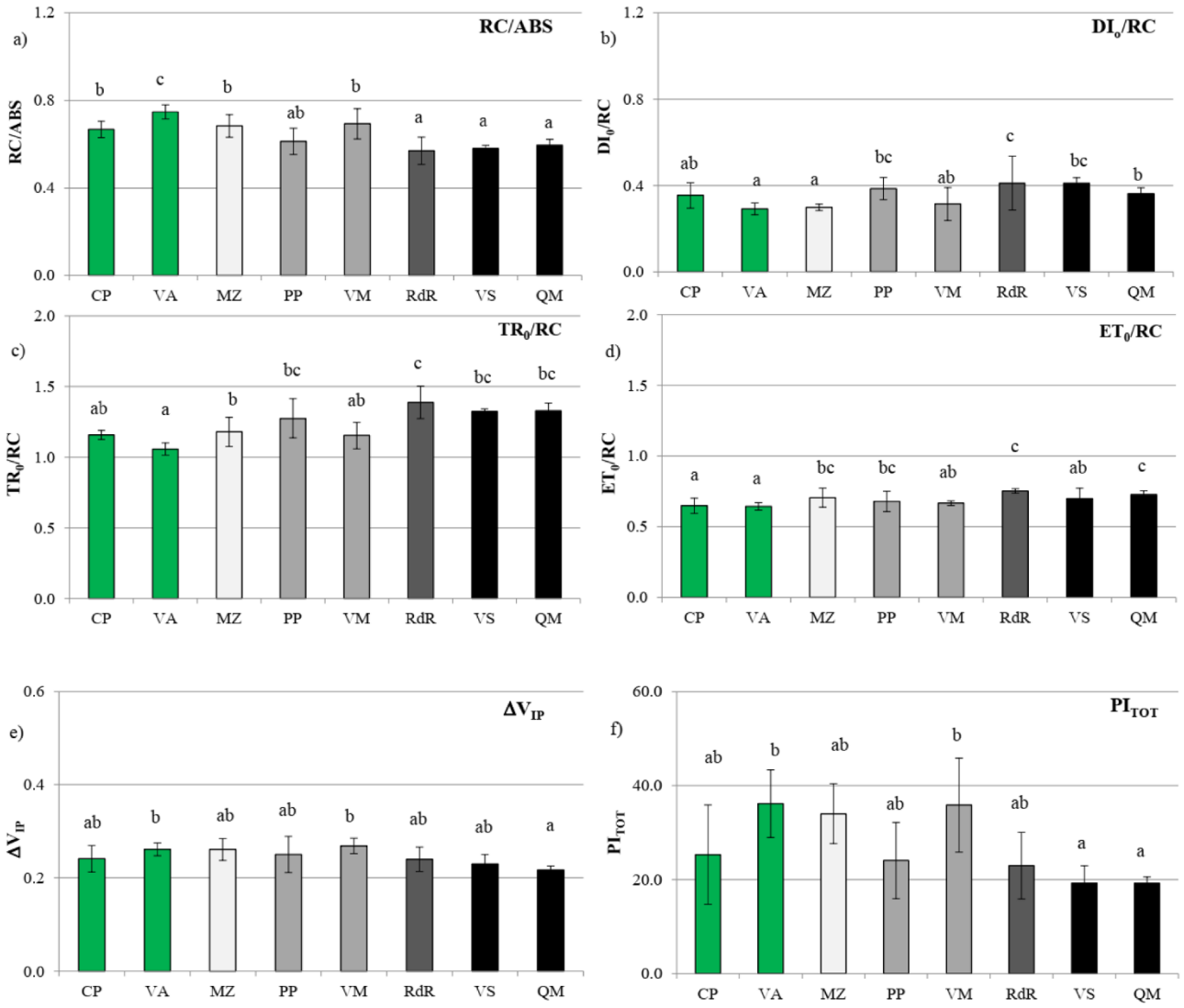


**Fig. 4.** JIP-test parameters in the experimental sites. The green bars indicated the two control sites: CP, Castelporziano and VA, Villa Ada urban park. Light, dark grey and black bars indicated sites with low, intermediate or higher magnetic susceptibility levels (see Fig. 2), respectively. A detailed sites description is reported in Material and Methods. Bars denote mean ± standard deviation (n = 4–5) and those not accompanied by the same letters are significantly different at $p < 0.05$. (For interpretation of the references to colour in this figure legend, the reader is referred to the web version of this article.)

where PM accumulated on leaves was higher, like RdR, VS and QM (Fig. 4 c, d). VA showed the lower value of both parameters whereas CP control site presented an intermediate value of $TR_0/RC$ and the lowest value of $ET_0/RC$, together with VA. Finally, $\Delta V_{IP}$ and $PI_{TOT}$ (Fig. 4 e, f) highlighted a pattern similar to RC/ABS among sites: VA, VM presented higher functionality of the IP phase and total photosynthetic performance, but in general, $\Delta V_{IP}$ presented slight differences among sites, with VA showed the maximum and QM the minimum. Following what was displayed by other parameters, CP did not present the trend of sites with lower magnetic susceptibility.

For a better understanding of the capacity of ChlF to discriminate the *Q. ilex* functionality in the different sites, PCA was applied. The sites with the high PM accumulation, grouped on the dark circle, are separated from the control sites, grey circle, whereas the sites with intermediate PM accumulation (MZ, PP, VM) have greater dispersion. RC/ABS, $PI_{TOT}$ and $\Delta V_{IP}$ are negatively related to Factor 1 (the factors' loading are −0.975, −0.915 and −0.777 respectively). Most of the records belonged to RdR, VS and QM are positively related to Factor 1, where $TR_0/RC$ and $DI_0/RC$ reached the higher loading (0.944 and 0.851 respectively) and records of those sites are negatively related to $ET_0/RC$ (−0.859 on Factor 2).

### 3.3. Chemical characterization

For each experimental site, Table 3 shows the concentrations of some of the more indicative analyzed elements in the soluble fraction of dust deposited on the leaves surface, and the results of OP measured through the AA assay. Concentrations of other analysed elements are reported in Appendix D. The differences among sites in terms of chemical elements' concentration followed a similar pattern for Cu, Fe, Mo, Sb and Sn, that are well-known tracers of non-emissive traffic contribution, such as brake and tire wear (Zhang et al., 2020). For these elements, in agreement with the magnetic measurements, the concentration at the traffic sites was higher than the one at the sites considered as control (CP, VA). The higher values were detected in RdR, VS and QM sites. The lowest values of K, La and Ce were measured only in CP and VA control sites, whereas MZ presented intermediate values together to PP, VM. The highest concentrations were detected in RdR, VS and QM. Pb showed the following trend: CP and VA < PP and VM < MZ < VS < RdR and QM, which differed from what was detected for the other chemical species. Lastly, the $OP^{AA}$ measurements of control sites (CP and VA) had the lower recorded values, while MZ, PP and VM showed intermediate values, in accordance with magnetic measures. RdR, VS and QM showed

**Table 3**
Chemical composition of the dust deposited on leaves: concentrations of some detected elements (ng $g^{-1}$) and the oxidative potential measured through the ascorbic acid assay ($OP^{AA}$; nmol AA $min^{-1}$ $g^{-1}$) assay. Values express mean ± standard deviation and those not accompanied by the same letters are significantly different at $p < 0.05$.

| Sites | Cu | Fe | Mo | Sb | Sn | Pb | K | La | Ce | $OP^{AA}$ |
|---|---|---|---|---|---|---|---|---|---|---|
| CP | 44 ± 10a | 1028 ± 218a | 2.1 ± 0.15a | 1.8 ± 0.39a | 1.1 ± 0.45a | 0.45 ± 0.03a | 53400 ± 6299a | 0.58 ± 0.51a | 1.3 ± 0.62a | 9.3 ± 2.97a |
| VA | 106 ± 8.1a | 1249 ± 100a | 2.6 ± 0.11a | 3.8 ± 0.82a | 0.69 ± 0.49a | 0.77 ± 0.68a | 63482 ± 4487bc | 0.53 ± 0.16a | 1.1 ± 0.11a | 12 ± 2.7a |
| MZ | 397 ± 75a | 2682 ± 84a | 8.1 ± 2.8a | 8.6 ± 2.3a | 5.7 ± 1.7a | 7.9 ± 5.6bc | 86126 ± 22835c | 1.2 ± 0.14a | 2.8 ± 0.92a | 38 ± 9.8b |
| PP | 496 ± 104a | 2406 ± 548a | 7.9 ± 2.1a | 9.8 ± 2.5a | 6.2 ± 1.2a | 5.6 ± 0.77b | 88057 ± 22835c | 1.4 ± 0.27a | 2.5 ± 0.42a | 49 ± 7.4b |
| VM | 409 ± 195a | 3255 ± 1818ab | 7.5 ± 1.9a | 7.9 ± 3.8a | 6.1 ± 2.9a | 3.8 ± 0.99b | 57929 ± 10881ab | 1.7 ± 0.44ab | 3.7 ± 1.3ab | 54 ± 12b |
| RdR | 1458 ± 274b | 5330 ± 626bc | 21 ± 5.2b | 19 ± 4.7b | 16 ± 2.5b | 16 ± 0.84e | 197979 ± 41003d | 2.1 ± 0.39bc | 4.4 ± 0.55bc | 153 ± 11c |
| VS | 1453 ± 568b | 6579 ± 2563c | 21 ± 6.9b | 26 ± 9.1b | 23 ± 10b | 10 ± 0.23cd | 139412 ± 57119cd | 2.6 ± 0.92c | 5.7 ± 1.9c | 166 ± 37c |
| QM | 1456 ± 218b | 6382 ± 328c | 20 ± 0.55b | 25 ± 1.6b | 17 ± 1.4b | 14 ± 3.2de | 137061 ± 22899cd | 3.7 ± 0.73d | 7.5 ± 0.73d | 204 ± 17d |

higher $OP^{AA}$ in the order RdR < VS < QM, following the findings of the susceptibility and chemical analysis.

The Pearson correlation analysis between JIP-test parameters, magnetic susceptibility and chemical species is shown in Tab. 4. When the correlation was significant, the selected JIP-test parameters are negatively correlated to the considered chemical elements and $OP^{AA}$ as well as to susceptibility except for $TR_0$/RC and $ET_0$/RC that showed a positive correlation. $DI_0$/RC did not show any correlation with the chemical and magnetic parameters, whereas RC/ABS, $\Delta V_{IP}$, $PI_{TOT}$ showed a negative correlation with Cu, Fe, Mo, Sb, Sn, Pb, La, K, Ce, $OP^{AA}$ and $\chi$. All the chemical elements increased with $\chi$, showing a direct correlation with a high r score between 0.977 and 0.686.

## 4. Discussion

PM is a major concern to human health and lately the attention on this pollutant increased, since it could be a co-factor that enhances the morbidity of infections such as the COVID-19 (Zoran et al., 2020). In Italy, vehicular traffic is responsible for about 40% of $PM_{10}$ emission (ISPRA, 2016), and its effects should be carefully monitored in cities like Rome, where the proportion between vehicles (including private cars and two-wheelers) and inhabitants is one of the highest in Europe, with roughly 75 vehicles × 100 inhabitants (Municipality of Rome, 2020).

The conventional PM monitoring methods employ high-cost instrumental stations that can frame the general PM concentration in different city context (Appendix A), but are not available for extensive sampling across the city (Norouzi et al., 2015), making important to develop an effective alternative monitoring activity of PM within urban areas with different traffic intensity. Monitoring approaches based on plants as biological indicators of air pollution can be a successful solution, as leaves have a high capability to intercept and accumulate PM (Przybysz et al., 2019). Most of the studies are focused on the capacity of plants to adsorb PM on leaves, whereas few works considered the functional damage that PM deposition may cause to urban vegetation (Han et al., 2020).

In the current study, *Q. ilex*, a native species also widespread in urban areas in Mediterranean Basin, has been used for biomonitoring of PM in different areas inside the Municipality of Rome. Several studies agree that *Q. ilex* is a good biomonitor for pollutants like ozone, polycyclic aromatic hydrocarbons (PAHs) (Alfani et al., 2001), but *Q. ilex* leaves can be effective in the absorption of particles as well through trichomes and leaf longevity that allow long-term loading of PM (Sgrigna et al., 2015). It has been well documented that the accumulation of particles on leaves depends on leaf characteristics such as hair density and wax content, leaf shape and morphology (Muhammad et al., 2020). Indeed an experiment on 96 plant species with contrasting morphological and anatomical leaf characteristics (Muhammad et al., 2019), showed that the highest leaf remanent magnetization by mass was observed on leaves of *Q. ilex* that was in the most effective group of net particle accumulators together with *Pseudotsuga menziesii*, *Thuja plicata*, *Juniperus communis*, *Picea pungens glauca* and *Rhododendron*.

Magnetic studies performed on leaves allow to discriminate the experimental sites providing useful information for a biomonitoring campaign from different points of view: PM accumulated on the leaf, emission sources and particle size (Sagnotti et al., 2009). The PM accumulated on leaves detected by magnetic susceptibility follows the PM air concentration gradient highlighted by mean annual values (Table 1), showing also the similarity between VA and MZ, in accordance to urban background air monitoring stations (Villa Ada and Cipro) that are close to these experimental sites (Appendix A and B).

Furthermore, magnetic measurements pointed out that sites with higher PM annual mean air concentration, such as VS or QM, show the highest magnetic susceptibility. In the other experimental sites (i.e. PP, VM, RdR), the magnetic susceptibility is lower and, accordingly, the amount of PM accumulated to the leaves too. Two concurrent issues can be used as an explanatory factor. On one side, the emissions related to vehicular traffic might be less intense (i.e. VM), on the other side, green infrastructures typologies, local urban settlement and road structure can strongly influence the dynamics of PM deposition on leaves (Łowicki, 2019; Qin et al., 2020). Indeed, in RdR, even close to Magna Grecia monitoring station, that shows the highest PM concentration along with Fermi in winter (Appendix A), dispersion could be favored relative to deposition and accumulation since in RdR the trees sampled are part of a circular line in a large open square, thus air circulation and dispersion of pollutants can be higher than in narrower street as VS or QM (Mei et al., 2018).

The hysteresis loops, that provide indications about the concentration, composition and grainsize of the magnetic particles, are all very similar between the sampled sites and differ mainly for the concentration-dependent magnetic parameters, thus suggesting that the variations of the magnetic properties are due to different concentration of magnetic minerals, which are similar for composition and grain size. The significant correlation between $\chi$, $M_S$ ($R^2 = 0.87$) and $M_{RS}$ ($R^2 = 0.81$), points out that all the concentration-dependent magnetic parameters are indicative of the same ferrimagnetic fraction, and that $\chi$, the easiest magnetic parameter to be measured, is suitable as an indicator of the concentration-dependent magnetic properties (Table 4). Indeed, the range of coercivity values, and other magnetic parameters such as the low values of the saturation field and the SIRM/$\chi$ values, all suggest that magnetite-like minerals are the main magnetic carriers, in agreement with former studies focused on the characterization of magnetic airborne particulate matter in Rome (Sagnotti et al., 2009).

In the Day plot, the magnetic particles of *Q. ilex* leaves fall in a region of the plot in-between the theoretical trends for SD-MD and SD-SP pure magnetites, near "brake" samples and far from "diesel" and "gasoline" exhausts, which instead follow the theoretical trends for mixtures of a single domain (SD) and multidomain (MD) magnetites (Sagnotti and Winkler, 2012, Appendix E). The Day plot highlights the possible coexistence of SP and SD/MD particles that might result from two processes in which the friction between a brake pad and the cast-iron brake disc produce Fe-bearing particles.

At brake pad temperatures below 200 °C, abrasive processes dominate, and wear particles >1 μm are mostly generated. At higher operational temperatures (>200 °C), the concentration of nanoparticles

**Table 4**
Pearson correlation analysis between JIP-test parameters, magnetic susceptibility and chemical species. The r-values underlined and highlighted in bold are significantly correlated at $p < 0.05$ and $p < 0.01$ respectively.

| | RC/ABS | $DI_0$/RC | $TR_0$/RC | $ET_0$/RC | $\Delta V_{IP}$ | $PI_{TOT}$ | Cu | Fe | Mo | Sb | Sn | Pb | K | La | Ce | $OP^{AA}$ | χ |
|---|---|---|---|---|---|---|---|---|---|---|---|---|---|---|---|---|---|
| RC/ABS | 1 | **−0.930** | **−0.984** | −0.770 | 0.762 | **0.906** | **−0.860** | −0.787 | **−0.857** | −0.826 | −0.838 | −0.816 | −0.828 | −0.713 | −0.704 | −0.815 | −0.755 |
| $DI_0$/RC | | 1 | **0.876** | 0.547 | −0.686 | **−0.888** | 0.722 | 0.624 | 0.709 | 0.677 | 0.723 | 0.615 | 0.730 | 0.485 | 0.482 | 0.652 | 0.595 |
| $TR_0$/RC | | | 1 | **0.863** | −0.717 | **−0.841** | **0.904** | 0.828 | **0.905** | **0.858** | **0.859** | **0.900** | **0.895** | 0.754 | 0.747 | **0.855** | 0.779 |
| $ET_0$/RC | | | | 1 | −0.523 | −0.541 | **0.851** | 0.781 | **0.869** | 0.783 | 0.759 | **0.984** | **0.914** | 0.718 | 0.725 | 0.801 | 0.668 |
| $\Delta V_{IP}$ | | | | | 1 | **0.928** | −0.741 | −0.699 | −0.705 | −0.755 | −0.715 | −0.608 | −0.617 | −0.729 | −0.719 | −0.798 | −0.751 |
| $PI_{TOT}$ | | | | | | 1 | −0.744 | −0.676 | −0.717 | −0.744 | −0.737 | −0.617 | −0.660 | −0.655 | −0.638 | −0.750 | −0.709 |
| Cu | | | | | | | 1 | **0.974** | **0.997** | **0.982** | **0.972** | **0.929** | **0.915** | **0.882** | **0.899** | **0.980** | **0.921** |
| Fe | | | | | | | | 1 | **0.976** | **0.986** | **0.980** | **0.868** | 0.811 | **0.928** | **0.954** | **0.977** | **0.962** |
| Mo | | | | | | | | | 1 | **0.979** | **0.976** | **0.939** | **0.916** | **0.874** | **0.896** | **0.970** | **0.909** |
| Sb | | | | | | | | | | 1 | **0.985** | **0.874** | **0.837** | **0.914** | **0.930** | **0.979** | **0.953** |
| Sn | | | | | | | | | | | 1 | **0.849** | **0.838** | **0.855** | **0.886** | **0.948** | **0.919** |
| Pb | | | | | | | | | | | | 1 | **0.949** | 0.795 | 0.804 | **0.887** | 0.773 |
| K | | | | | | | | | | | | | 1 | 0.659 | 0.676 | **0.841** | 0.695 |
| La | | | | | | | | | | | | | | 1 | **0.993** | **0.946** | **0.974** |
| Ce | | | | | | | | | | | | | | | 1 | **0.956** | **0.977** |
| $OP^{AA}$ | | | | | | | | | | | | | | | | 1 | **0.966** |
| χ | | | | | | | | | | | | | | | | | 1 |

(<100 nm) increases due to evaporation, condensation and aggregation processes, increasing by four to six orders of magnitude the emission rate of particles, thus constituting >90% of total brake dust and constituting a major source of airborne magnetic nanoparticles (Gonet and Maher, 2019).

However, the obtained results tend to corroborate the first emissive process: none of the magnetic properties diagnostic of the relevant presence of ultrafine SP particles, e.g. the enhancement of magnetic susceptibility, and low SIRM/χ values, supported the presence of ultrafine magnetic particles. Moreover, in traffic-related PM, a SP behavior may occur as coating of MD particles and is originated by localized stress in the oxidized outer shell surrounding the unoxidized core of magnetite-like grains; thus it cannot be considered as a direct proxy for the overall content of ultrafine <30 nm particles (Sagnotti and Winkler, 2012).

This result can explain why morpho-functional traits as chlorophyll concentration ($Chl_{SPAD}$) or relative water content (RWC), which are mostly damaged by ultrafine particles able to penetrate inside the leaves through stomata, were not affected in our case (Rai, 2016). RWC was inside the range of good hydration for *Quercus* species (Salvatori et al., 2016) indicating that, in the conditions experienced in this study, PM deposited and accumulated on leaves is not a determinant factor in plant water status. Overall, it is not possible to exclude the presence of ultrafine SP particles, since they are more difficult to be recognized with standard room temperature magnetic measurements, for their intrinsically unstable magnetic properties.

The results of the current study reinforce the evidence that leaves are suitable indicators of the non-combustible fraction of PM, following what has been found by former studies (Winkler et al., 2020). Indeed, the hysteresis ratio values of the sampled leaves fall in the same cluster defined in other experimental activities carried out on lichens transplanted in Milan, *Q. ilex* leaves sampled in Rome, Italy, as well as in previous experimental campaigns, or PM filters and dust arising from fuel exhausts and brakes' emissions (Appendix E). To confirm this interpretation, we notice that the SIRM/χ values (5.3 ± 1.0 kA/m) are compatible with those typical of the brake emissions (6.7 ± 2.5 kA/m) and distinct from those typical for gasoline and diesel exhaust emissions (13.8 ± 6.3 kA/m and 14.5 ± 12.1 kA/m, respectively) as reviewed in Gonet and Maher, 2019.

On the other hand, vehicle brake wear was by far the most dominant source of airborne magnetite in the roadside environment of two sites in UK, being responsible for between ~68 and 85% of the total airborne magnetite content (Gonet et al., 2021), thus confirming that non-exhaust sources of vehicular traffic, notably brake abrasion, are the main driver of PM air pollution in urban contexts. In conformity to hysteresis properties and results from other studies, magnetic susceptibility is positively correlated with non-exhaustive traffic source tracers as Cu, Fe, Mo, Sb, Sn, Pb (Hofman et al., 2017). The mixed nature of PM metals detected on leaves underlined the role of vehicular traffic as one of the main sources of PM pollution in large cities (Amato et al., 2013). La, K, and Ce that are usually more related to road dust, constituted also by soil dust (Simonetti et al., 2018), increased from control to more polluted sites, suggesting that passing traffic facilitates resuspension of soil particles that had been deposited on roads (Hasheminassab et al., 2020).

PM impact on vegetation is often underestimated but can play a pivotal role in plant physiology through direct and indirect damages (Rai, 2016). Among morpho-functional traits, SLA did not show variations attributable to PM. However, control sites have higher sclerophyll degree (lower SLA values) due to inherent ecological conditions as solar radiation, supporting plants in counteracting the oxidative stress since lower SLA means higher responsiveness and high photosynthesis capacity per surface unit supporting efficient detoxification processes (Bussotti, 2008). On the other side this morpho-functional trait influence directly the biomonitoring activity of PM in as much as lower leaf area means less PM accumulation capacity (Sæbø et al., 2012). In our

experiment, $Chl_{SPAD}$ remained almost constant through the different sites, even in those with high PM accumulation. Despite this result, photosystems functionality was affected by PM exposure decreasing as PM on leaves increased. We hypothesize that PM alters the optical properties of leaves reducing the incident photosynthetically active radiation (PAR) on the leaf surface, because of changes in the reflectance in the visible and short wave infrared radiation (Popek et al., 2018; Rai, 2016). RC/ABS that provides information about the first photochemical reactions in the antenna and on PSII acceptor side, highlights a decreasing amount of electrons flow. RC/ABS decreases because of several processes as photoinhibition, downregulation, or shading adaptation (Pavlík et al., 2012). When the light energy is not appropriately transferred to electron transport, the photosynthetic apparatus suffers an overexcitation and thus RC/ABS decreases. However, this down-regulation mechanism entails an increase of the energy dissipation as heat, $DI_0/RC$ (Pollastrini et al., 2020; Salvatori et al., 2013), that we do not observe in our case study. Analysing the changes within the constellation of parameters obtained from the JIP-test, shading adaptation seems the prevalent mechanism. PM accumulated on the adaxial surface absorbs and scatter light, and shading condition results in a physiological acclimation with an increase of the antenna size that can cause a decrease of RC/ABS via increasing of Chl to RC (Valladares and Niinemets, 2008). It is worth notice that $TR_0/RC$ and $ET_0/RC$ are directly correlated with $\chi$, i.e. increased with the PM accumulation, meaning that as a compensatory mechanism, the decrease of the incoming electron flow implies an increase of trapping and electron transport flow beyond the $QA^-$ per active RC. The trend of $PI_{TOT}$, that decrease in RdR, VS and QM sites, was connected to its component RC/ABS, but also to the decreased capacity to reduce the final electron acceptors beyond PSI ($\Delta V_{IP}$) that is lower in the sites most exposed to PM. RC/ABS, $PI_{TOT}$ and $\Delta V_{IP}$ are effective in discriminating sites in line with their low (CP, VA) or high (RdR, VS and QM) PM accumulation as showed by PCA (Fig. 5), whereas, the higher dispersion of MZ, VM and PP data, might be related to site-specific conditions that can affect photosystems functionality increasing the variability of physiological response (Medrano et al., 2009). In general, this data could be explained by a general increase of oxidative potential with PM accumulation on leaves. PM can generate oxidative stress depending on its chemical nature, since the heavy metals present in road-side PM can affect leaf pH, antioxidant activity or pigments content and the related functional processes (Rai, 2016 and references therein). The chemical elements present in PM, can induce the cellular generation of reactive oxygen species (Gao et al., 2020) and this PM capability can be evaluated through ascorbic acid assay, an effective approach to estimating the ecotoxicology of particles. As already demonstrated through PM sampled on filters, $OP^{AA}$ values were strongly correlated with tracers of brake dust abrasion, confirming the high sensitivity of this assay towards non-emissive traffic contribution, even in the case of PM deposited on leaves (Moufarrej et al., 2020). Indeed, between $OP^{AA}$ and $\chi$ there is a tight correlation confirming that also in leaves soluble Fe is strongly associated with ROS activity as found by Cheung et al., 2010 on filters.

*Quercus ilex* has been proven a tolerant species to moderate oxidative stress, able to respond to ROS production enhancing the antioxidant defence through different mechanisms (Fusaro et al., 2017b; Hasanuzzaman et al., 2020). The first enzymatic defence involves the activation of Super Oxide Dismutase (SOD) that consumes the redox potential used for reducing end acceptors of PSI and accordingly producing a $\Delta V_{IP}$ decrease even if the trapping capacity and electron transport rate increase per active reaction centre. It is interesting to notice that the elements that can have higher oxidative stress potential on vegetation, such as Cu, Fe, Mo, Pb (Bernardini et al., 2016) have not shown substantial differences in concentration between RdR, VS and QM, that anyway present different amount of total PM accumulated ($\chi$ = RdR < VS < QM). Thus, the variation of functional indicators relative to PSI seems to respond to the chemical species concentration, as for Al and Zn are double of what was measured in the others sites (Appendix D), and $\Delta V_{IP}$ and $PI_{TOT}$ showed a higher correlation with $OP^{AA}$ than $\chi$. Beyond this general framework, established under the obtained results, the low performance of CP registered although the small PM accumulation, can depend on natural stress as sea spry and soil salinity that inherently insist on this control site in the winter period, as has been found in previous studies in that area (Fusaro et al., 2019a, 2019b; Mereu et al., 2009). Indeed, ChlF parameters in CP site highlight a general low performance of photosystems in processing energy incoming rather than a specific action of stress on PSII or PSI, highlighting chronic stress on photosystems functionality in that natural site.

## 5. Conclusions

In the present study, several morpho-functional traits were measured to find out the most effective indicators of PM impairment on plant functionality. Among the analysed morpho-functional traits, photosystem functionality, measured by prompt fluorescence of chlorophyll, is the most suitable to detect the PM effects. In our case study, PM does not produce an alteration of plant water status or structural damage to pigments, whereas ChlF highlights two mechanisms of action. On the

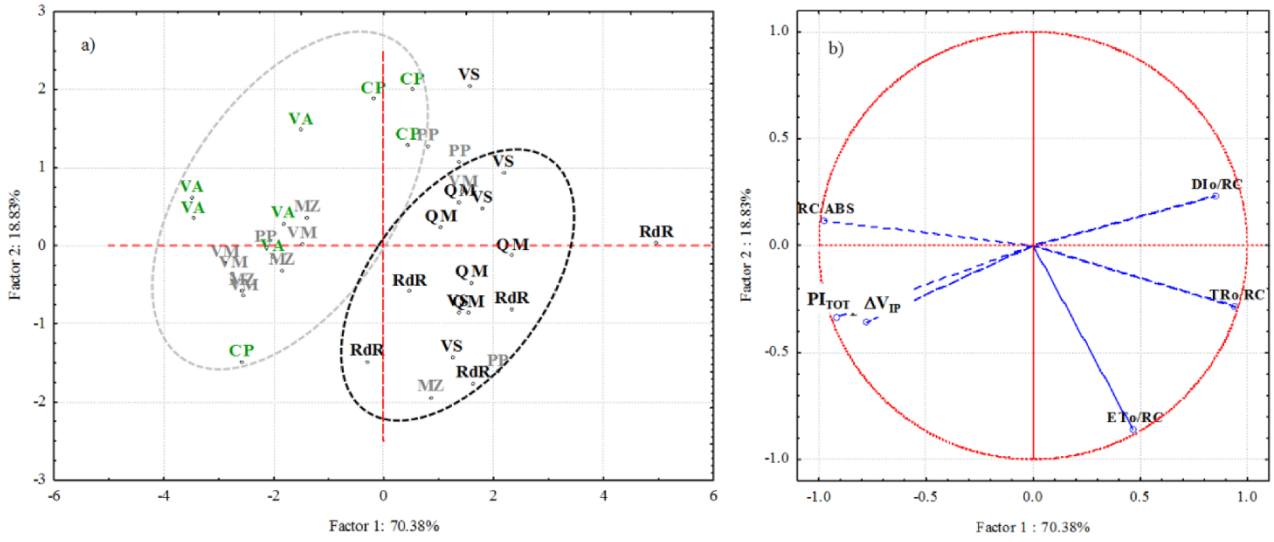


**Fig. 5.** Principal Component Analysis of the studied sites based on JIP-test parameters (RC/ABS, $DI_0/RC$, $TR_0/RC$, $ET_0/RC$, $\Delta V_{IP}$, $PI_{TOT}$) (a) and factors' loadings (b). For each site, the replicates (sampled trees) are reported.

PSII side, the shading effect is prevalent on *Q. ilex*, and RC/ABS can be used as a good indicator of PM accumulated on the leaf surface. On PSI side, the concentration of chemical species might drive a slight impact on PSI functionality and thus on carbon assimilation, since the decrease in the relative contribution of electron flow to the PSI end acceptors ($\Delta V_{IP}$) is present. This result can be linked to oxidative stress imposed by PM and detected by an ascorbic acid trial (OP). Correlation between indicators obtained from different approaches pointed out that $PI_{TOT}$ and $DI_0$/RC can respond also to other oxidative stressors than PM since they are less or not correlated at all to the magnetic susceptibility and elemental content concentration as well.

The magnetic susceptibility measured on *Q. ilex* leaves is confirmed to be a robust proxy for the bioaccumulation of trace metals, since its tight positive correlation with chemical species detected on leaves. Magnetic and chemical analyses, in conformity with previous studies in the urban area, highlighted that non-exhaust traffic emission (i.e. brake abrasion) are the main sources of the magnetic and metallic fraction of PM bioaccumulated on leaves in the proximity of roads. Leaves provide useful information about PM accumulation that can be uncoupled to PM air concentration because the deposition process on leaves surface can be influenced by green infrastructures typologies and street aerodynamic features. Leaves frame a long-term exposure to PM, the more appropriate dimension to evaluate its effects on urban vegetation functionality and the negative feedback on the provisioning of ecosystem services.

Experimental activities should be promoted on species that are more sensitive than *Q. ilex* that shows an adaptive response to PM stress for low to intermediate accumulation, having functional damage only for high PM on leaves. If this species is highly suggested to stakeholders as a key element of green infrastructure finalized to PM removal due to its high bioaccumulation potential and functional tolerance, it is not suitable for monitoring variation of functionality linked to the effects of low air quality in our city.

A multidisciplinary biomonitoring activity comprehensive of a large number of urban sites should be promoted to detect emission sources and distribution patterns of airborne persistent pollutants when it is impossible to apply a high-density instrumental monitoring of PM.

## CRediT authorship contribution statement

**Lina Fusaro:** Conceptualization, Methodology, Investigation, Formal analysis, Data curation, Visualization, Writing - original draft, Writing - review & editing. **Elisabetta Salvatori:** Conceptualization, Methodology, Investigation, Visualization, Writing - original draft, Writing - review & editing. **Aldo Winkler:** Methodology, Investigation, Writing - original draft, Writing - review & editing. **Maria Agostina Frezzini:** Investigation, Resources, Writing - review & editing. **Elena De Santis:** Investigation, Resources. **Leonardo Sagnotti:** Methodology, Writing - review & editing, Supervision, Funding acquisition. **Silvia Canepari:** Writing - review & editing, Supervision, Funding acquisition. **Fausto Manes:** Conceptualization, Methodology, Writing - review & editing, Supervision, Funding acquisition.

## Declaration of Competing Interest

The authors declare that they have no known competing financial interests or personal relationships that could have appeared to influence the work reported in this paper.

## Acknowledgements

This work was supported by Accademia delle Scienze detta dei XL [grant 2018]; Sapienza Ateneo Research Project 2019 [Prot. Num. RM11916B79293E6F].

## Appendix A. Supplementary data

Supplementary data to this article can be found online at https://doi.org/10.1016/j.ecolind.2021.107707.

## References

Alessio, M., Anselmi, S., Conforto, L., Improta, S., Manes, F., Manfra, L., 2002. Radiocarbon as a biomarker of urban pollution in leaves of evergreen species sampled in Rome and in rural areas (Lazio—Central Italy). Atmos. Environ. 36 (34), 5405–5416. https://doi.org/10.1016/S1352-2310(02)00409-0.

Alfani, A., Maisto, G., Vittoria Prati, M., Baldantoni, D., 2001. Leaves of *Quercus ilex* L. as biomonitors of PAHs in the air of Naples (Italy). Atmos. Environ. 35 (21), 3553–3559. https://doi.org/10.1016/S1352-2310(01)00087-5.

Amato, F., Schaap, M., Reche, C., Querol, X., 2013. Road traffic: a major source of particulate matter in Europe. In: Viana, M. (Ed.), Urban Air Quality in Europe, The Handbook of Environmental Chemistry. Springer, Berlin, Heidelberg, pp. 165–193, 10.1007/698_2012_211.

Bates, J.T., Fang, T., Verma, V., Zeng, L., Weber, R.J., Tolbert, P.E., Abrams, J.Y., Sarnat, S.E., Klein, M., Mulholland, J.A., Russell, A.G., 2019. Review of acellular assays of ambient particulate matter oxidative potential: methods and relationships with composition, sources, and health effects. Environ. Sci. Technol. 53 (8), 4003–4019. https://doi.org/10.1021/acs.est.8b03430.

Bernardini, A., Salvatori, E., Guerrini, V., Fusaro, L., Canepari, S., Manes, F., 2016. Effects of high Zn and Pb concentrations on *Phragmites australis* (Cav.) Trin. Ex. Steudel: photosynthetic performance and metal accumulation capacity under controlled conditions. Int. J. Phytorem. 18 (1), 16–24. https://doi.org/10.1080/15226514.2015.1058327.

Blanusa, T., Fantozzi, F., Monaci, F., Bargagli, R., 2015. Leaf trapping and retention of particles by holm oak and other common tree species in Mediterranean urban environments. Urban For. Urban Greening 14 (4), 1095–1101. https://doi.org/10.1016/j.ufug.2015.10.004.

Bolund, P., Hunhammar, S., 1999. Ecosystem services in urban areas. Ecol. Econ. 29 (2), 293–301. https://doi.org/10.1016/S0921-8009(99)00013-0.

Bussotti, F., 2008. Functional leaf traits, plant communities and acclimation processes in relation to oxidative stress in trees: a critical overview. Glob. Change Biol. 14, 2727–2739. https://doi.org/10.1111/j.1365-2486.2008.01677.x.

Bussotti, F., Pollastrini, M., 2015. Evaluation of leaf features in forest trees: methods, techniques, obtainable information and limits. Ecol. Ind. 52, 219–230. https://doi.org/10.1016/j.ecolind.2014.12.010.

Campbell, S.J., Utinger, B., Lienhard, D.M., Paulson, S.E., Shen, J., Griffiths, P.T., Stell, A. C., Kalberer, M., 2019. Development of a physiologically relevant online chemical assay to quantify aerosol oxidative potential. Anal. Chem. 91 (20), 13088–13095. https://doi.org/10.1021/acs.analchem.9b03282.

Canepari, S., Cardarelli, E., Perrino, C., Catrambone, M., Pietrodangelo, A., Strincone, M., 2006. Two-stage chemical fractionation method for the analysis of elements and non-volatile inorganic ions in $PM_{10}$ samples: application to ambient samples collected in Rome (Italy). Atmos. Environ. 40 (40), 7908–7923. https://doi.org/10.1016/j.atmosenv.2006.07.005.

Canepari, S., Pietrodangelo, A., Perrino, C., Astolfi, M.L., Marzo, M.L., 2009. Enhancement of source traceability of atmospheric PM by elemental chemical fractionation. Atmos. Environ. Urban Air Qual. 43, 4754–4765. https://doi.org/10.1016/j.atmosenv.2008.09.059.

Chaparro, M.A.E., Chaparro, M.A.E., Castañeda-Miranda, A.G., Marié, D.C., Gargiulo, J. D., Lavornia, J.M., Natal, M., Böhnel, H.N., 2020. Fine air pollution particles trapped by street tree barks: in situ magnetic biomonitoring. Environ. Pollut. 266, 115229. https://doi.org/10.1016/j.envpol.2020.115229.

Cheung, K.L., Ntziachristos, L., Tzamkiozis, T., Schauer, J.J., Samaras, Z., Moore, K.F., Sioutas, C., 2010. Emissions of particulate trace elements, metals and organic species from gasoline, diesel, and biodiesel passenger vehicles and their relation to oxidative potential. Aerosol Sci. Technol. 44 (7), 500–513. https://doi.org/10.1080/02786821003758294.

Comunian, S., Dongo, D., Milani, C., Palestini, P., 2020. Air pollution and COVID-19: the role of particulate matter in the spread and increase of COVID-19's morbidity and mortality. Int. J. Environ. Res. Public Health 17, 4487. https://doi.org/10.3390/ijerph17124487.

Conticini, E., Frediani, B., Caro, D., 2020. Can atmospheric pollution be considered a co-factor in extremely high level of SARS-CoV-2 lethality in Northern Italy? Environ. Pollut. 261, 114465. https://doi.org/10.1016/j.envpol.2020.114465.

Costabile, F., Gualtieri, M., Ancona, C., Canepari, S., Decesari, S., 2020. Ultrafine particle features associated with pro-inflammatory and oxidative responses: implications for health studies. Atmosphere 11, 414. https://doi.org/10.3390/atmos11040414.

Day, R., Fuller, M., Schmidt, V.A., 1977. Hysteresis properties of titanomagnetites: grain-size and compositional dependence. Phys. Earth Planet. Inter. 13 (4), 260–267. https://doi.org/10.1016/0031-9201(77)90108-X.

Desotgiu, R., Cascio, C., Pollastrini, M., Gerosa, G., Marzuoli, R., Bussotti, F., 2012. Short and long term photosynthetic adjustments in sun and shade leaves of *Fagus sylvatica* L., investigated by fluorescence transient (FT) analysis. Plant Biosyst. Int. J. Aspects Plant Biol. 146 (sup1), 206–216. https://doi.org/10.1080/11263504.2012.705350.

Dunlop, D.J., 2002a. Theory and application of the Day plot ($M_{rs}/M_s$ versus $H_{cr}/H_c$) 1. Theoretical curves and tests using titanomagnetite data. J. Geophys. Res. 107, 2056. https://doi.org/10.1029/2001JB000486.

Dunlop, D.J., 2002b. Theory and application of the Day plot (Mrs/Ms versus Hcr/Hc) 2. Application to data for rocks, sediments, and soils. J. Geophys. Res. (Solid Earth) 107, 2057. https://doi.org/10.1029/2001JB000487.

Fattorini, D., Regoli, F., 2020. Role of the chronic air pollution levels in the Covid-19 outbreak risk in Italy. Environ. Pollut. 264, 114732. https://doi.org/10.1016/j.envpol.2020.114732.

Ficociello, G., Inverni, A., Massimi, L., Buccini, G., Canepari, S., Uccelletti, D., 2020. Assessment of the effects of atmospheric pollutants using the animal model *Caenorhabditis elegans*. Environ. Res. 191, 110209. https://doi.org/10.1016/j.envres.2020.110209.

Flanders, P.J., 1994. Collection, measurement, and analysis of airborne magnetic particulates from pollution in the environment (invited). J. Appl. Phys. 75 (10), 5931–5936. https://doi.org/10.1063/1.355518.

Frezzini, M.A., Castellani, F., De Francesco, N., Ristorini, M., Canepari, S., 2019. Application of DPPH assay for assessment of particulate matter reducing properties. Atmosphere 10, 816. https://doi.org/10.3390/atmos10120816.

Fusaro, L., Marando, F., Sebastiani, A., Capotorti, G., Blasi, C., Copiz, R., Congedo, L., Munafò, M., Ciancarella, L., Manes, F., 2017a. Mapping and assessment of $PM_{10}$ and $O_3$ removal by woody vegetation at urban and regional level. Remote Sensing 9, 791. https://doi.org/10.3390/rs9080791.

Fusaro, L., Mereu, S., Salvatori, E., Spano, D., Manes, F., 2019a. Drought stress affects temperature response of leaf dark respiration in mediterranean coastal maquis species. Annali di Botanica 9, 39–52. https://doi.org/10.13133/2239-3129/14621.

Fusaro, L., Palma, A., Salvatori, E., Basile, A., Maresca, V., Asadi Karam, E., Manes, F., Aceto, S., 2017b. Functional indicators of response mechanisms to nitrogen deposition, ozone, and their interaction in two Mediterranean tree species. PLoS ONE 12 (10). https://doi.org/10.1371/journal.pone.0185836 e0185836.

Fusaro, L., Salvatori, E., Mereu, S., Manes, F., 2019b. Photosynthetic traits as indicators for phenotyping urban and peri-urban forests: a case study in the metropolitan city of Rome. Ecol. Ind. 103, 301–311. https://doi.org/10.1016/j.ecolind.2019.04.033.

Gao, D., Ripley, S., Weichenthal, S., Godri Pollitt, K.J., 2020. Ambient particulate matter oxidative potential: Chemical determinants, associated health effects, and strategies for risk management. Free Radical Biol. Med. Air Poll.: Consequences Cellular Redox Signaling, Antioxidant Defenses Dis. 151, 7–25. https://doi.org/10.1016/j.freeradbiomed.2020.04.028.

Georgeaud, V.M., Rochette, P., Ambrosi, J.P., Vandamme, D., Williamson, D., 1997. Relationship between heavy metals and magnetic properties in a large polluted catchment: the Etang de Berre (south of France). Phys. Chem. Earth. 22 (1-2), 211–214. https://doi.org/10.1016/S0079-1946(97)00105-5.

Gonet, T., Maher, B.A., 2019. Airborne, vehicle-derived Fe-bearing nanoparticles in the urban environment: a review. Environ. Sci. Technol. 53 (17), 9970–9991. https://doi.org/10.1021/acs.est.9b01505.

Gonet, T., Maher, B.A., Kukutschová, J., 2021. Source apportionment of magnetite particles in roadside airborne particulate matter. Sci. Total Environ. 752, 141828. https://doi.org/10.1016/j.scitotenv.2020.141828.

Grote, R., Samson, R., Alonso, R., Amorim, J.H., Cariñanos, P., Churkina, G., Fares, S., Thiec, D.L., Niinemets, Ü., Mikkelsen, T.N., Paoletti, E., Tiwary, A., Calfapietra, C., 2016. Functional traits of urban trees: air pollution mitigation potential. Front. Ecol. Environ. 14 (10), 543–550. https://doi.org/10.1002/fee.1426.

Han, D., Shen, H., Duan, W., Chen, L., 2020. A review on particulate matter removal capacity by urban forests at different scales. Urban For. Urban Green. 48, 126565. https://doi.org/10.1016/j.ufug.2019.126565.

Hasanuzzaman, M., Bhuyan, M.H.M.B., Zulfiqar, F., Raza, A., Mohsin, S.M., Mahmud, J. A., Fujita, M., Fotopoulos, V., 2020. Reactive oxygen species and antioxidant defense in plants under abiotic stress: revisiting the crucial role of a universal defense regulator. Antioxidants 9, 681. https://doi.org/10.3390/antiox9080681.

Hasheminassab, S., Sowlat, M.H., Pakbin, P., Katzenstein, A., Low, J., Polidori, A., 2020. High time-resolution and time-integrated measurements of particulate metals and elements in an environmental justice community within the Los Angeles Basin: Spatio-temporal trends and source apportionment. Atmospheric Environ: X 7, 100089. https://doi.org/10.1016/j.aeaoa.2020.100089.

Hoffmann, V., Knab, M., Appel, E., 1999. Magnetic susceptibility mapping of roadside pollution. J. Geochem. Explor. 66 (1-2), 313–326. https://doi.org/10.1016/S0375-6742(99)00014-X.

Hofman, J., Maher, B.A., Muxworthy, A.R., Wuyts, K., Castanheiro, A., Samson, R., 2017. Biomagnetic monitoring of atmospheric pollution: a review of magnetic signatures from biological sensors. Environ. Sci. Technol. 51 (12), 6648–6664. https://doi.org/10.1021/acs.est.7b00832.

Hunt, A., Jones, J., Oldfield, F., 1984. Magnetic measurements and heavy metals in atmospheric particulates of anthropogenic origin. Sci. Total Environ., Highway Pollut. 33 (1-4), 129–139. https://doi.org/10.1016/0048-9697(84)90387-5.

Janhäll, S., 2015. Review on urban vegetation and particle air pollution – deposition and dispersion. Atmos. Environ. 105, 130–137. https://doi.org/10.1016/j.atmosenv.2015.01.052.

Jordanova, D., Hoffmann, V., Fehr, K.T., 2004. Mineral magnetic characterization of anthropogenic magnetic phases in the Danube river sediments (Bulgarian part). Earth Planet. Sci. Lett. 221 (1-4), 71–89. https://doi.org/10.1016/S0012-821X(04)00074-3.

Kapper, K.L., Bautista, F., Goguitchaishvili, A., Bógalo, M.F., Cejudo-Ruíz, R., Cervantes Solano, M., 2020. The use and misuse of magnetic methods to monitor environmental pollution in urban areas – Uso y abuso de métodos magnéticos en el monitoreo de contaminación ambiental en áreas urbanas. Bolet. Sociedad Geológica Mexicana 72 (1). https://doi.org/10.18268/BSGM10.18268/BSGM2020v72n110.18268/BSGM2020v72n1a111219.

Łowicki, D., 2019. Landscape pattern as an indicator of urban air pollution of particulate matter in Poland. Ecol. Ind. 97, 17–24. https://doi.org/10.1016/j.ecolind.2018.09.050.

Manes, F., Marando, F., Capotorti, G., Blasi, C., Salvatori, E., Fusaro, L., Ciancarella, L., Mircea, M., Marchetti, M., Chirici, G., Munafò, M., 2016. Regulating ecosystem services of forests in ten italian metropolitan cities: air quality improvement by $PM_{10}$ and $O_3$ removal. Ecol. Ind. 67, 425–440. https://doi.org/10.1016/j.ecolind.2016.03.009.

Massimi, L., Ristorini, M., Astolfi, M.L., Perrino, C., Canepari, S., 2020. High resolution spatial mapping of element concentrations in PM10: a powerful tool for localization of emission sources. Atmos. Res. 244, 105060. https://doi.org/10.1016/j.atmosres.2020.105060.

Medrano, H., Flexas, J., Galmés, J., 2009. Variability in water use efficiency at the leaf level among Mediterranean plants with different growth forms. Plant Soil 317 (1-2), 17–29. https://doi.org/10.1007/s11104-008-9785-z.

Mei, D., Wen, M., Xu, X., Zhu, Y., Xing, F., 2018. The influence of wind speed on airflow and fine particle transport within different building layouts of an industrial city. J. Air Waste Manag. Assoc. 68 (10), 1038–1050. https://doi.org/10.1080/10962247.2018.1465487.

Mereu, S., Salvatori, E., Fusaro, L., Gerosa, G., Muys, B., Manes, F., 2009. A whole plant approach to evaluate the water use of mediterranean maquis species in a coastal dune ecosystem. Biogeosci. Discuss. 6, 1713–1746. https://doi.org/10.5194/bgd-6-1713-2009.

Moreno, E., Sagnotti, L., Dinarès-Turell, J., Winkler, A., Cascella, A., 2003. Biomonitoring of traffic air pollution in Rome using magnetic properties of tree leaves. Atmos. Environ. 37 (21), 2967–2977. https://doi.org/10.1016/S1352-2310(03)00244-9.

Moufarrej, L., Courcot, D., Ledoux, F., 2020. Assessment of the PM2.5 oxidative potential in a coastal industrial city in Northern France: relationships with chemical composition, local emissions and long range sources. Sci. Total Environ. 748, 141448. https://doi.org/10.1016/j.scitotenv.2020.141448.

Muhammad, S., Wuyts, K., Samson, R., 2020. Immobilized atmospheric particulate matter on leaves of 96 urban plant species. Environ. Sci. Pollut. Res. 27 (29), 36920–36938. https://doi.org/10.1007/s11356-020-09246-6.

Muhammad, S., Wuyts, K., Samson, R., 2019. Atmospheric net particle accumulation on 96 plant species with contrasting morphological and anatomical leaf characteristics in a common garden experiment. Atmos. Environ. 202, 328–344. https://doi.org/10.1016/j.atmosenv.2019.01.015.

Mukherjee, A., Agrawal, M., 2018. Use of GLM approach to assess the responses of tropical trees to urban air pollution in relation to leaf functional traits and tree characteristics. Ecotoxicol. Environ. Saf. 152, 42–54. https://doi.org/10.1016/j.ecoenv.2018.01.038.

Norouzi, S., Khademi, H., Faz Cano, A., Acosta, J.A., 2015. Using plane tree leaves for biomonitoring of dust borne heavy metals: a case study from Isfahan, Central Iran. Ecol. Ind. 57, 64–73. https://doi.org/10.1016/j.ecolind.2015.04.011.

Nowak, D.J., Crane, D.E., Stevens, J.C., 2006. Air pollution removal by urban trees and shrubs in the United States. Urban For. Urban Greening 4 (3-4), 115–123. https://doi.org/10.1016/j.ufug.2006.01.007.

Orioli Riccardo, Antonucci Chiara, Scortichini Matteo, Cerza Francesco, Marando Federica, Ancona Carla, Manes Fausto, Davoli Marina, Michelozzi Paola, Forastiere Francesco, Cesaroni Giulia, n.d. Exposure to Residential Greenness as a Predictor of Cause-Specific Mortality and Stroke Incidence in the Rome Longitudinal Study. Environmental Health Perspectives 127, 027002. https://doi.org/10.1289/EHP2854.

Pavlík, M., Pavlíková, D., Zemanová, V., Hnilička, F., Urbanová, V., Száková, J., 2012. Trace elements present in airborne particulate matter—stressors of plant metabolism. Ecotoxicol. Environ. Saf. 79, 101–107. https://doi.org/10.1016/j.ecoenv.2011.12.009.

Piacentini, D., Falasca, G., Canepari, S., Massimi, L., 2019. Potential of PM-selected components to induce oxidative stress and root system alteration in a plant model organism. Environ. Int. 132, 105094. https://doi.org/10.1016/j.envint.2019.105094.

Pietrogrande, M.C., Russo, M., Zagatti, E., 2019. Review of PM oxidative potential measured with acellular assays in urban and rural sites across Italy. Atmosphere 10, 626. https://doi.org/10.3390/atmos10100626.

Pollastrini, M., Salvatori, E., Fusaro, L., Manes, F., Marzuoli, R., Gerosa, G., Brüggemann, W., Strasser, R.J., Bussotti, F., 2020. Selection of tree species for forests under climate change: is PSI functioning a better predictor for net photosynthesis and growth than PSII? Tree Physiol. 40, 1561–1571. https://doi.org/10.1093/treephys/tpaa084.

Popek, R., Przybysz, A., Gawrońska, H., Klamkowski, K., Gawroński, S.W., 2018. Impact of particulate matter accumulation on the photosynthetic apparatus of roadside woody plants growing in the urban conditions. Ecotoxicol. Environ. Saf. 163, 56–62. https://doi.org/10.1016/j.ecoenv.2018.07.051.

Przybysz, A., Nersisyan, G., Gawroński, S.W., 2019. Removal of particulate matter and trace elements from ambient air by urban greenery in the winter season. Environ. Sci. Pollut. Res. 26 (1), 473–482.

Qin, H., Hong, B.o., Huang, B., Cui, X., Zhang, T., 2020. How dynamic growth of avenue trees affects particulate matter dispersion: CFD simulations in street canyons. Sustainable Cit. Soc. 61, 102331. https://doi.org/10.1016/j.scs.2020.102331.

Rai, P.K., 2016. Impacts of particulate matter pollution on plants: Implications for environmental biomonitoring. Ecotoxicol. Environ. Saf. 129, 120–136. https://doi.org/10.1016/j.ecoenv.2016.03.012.

Sæbø, A., Popek, R., Nawrot, B., Hanslin, H.M., Gawronska, H., Gawronski, S.W., 2012. Plant species differences in particulate matter accumulation on leaf surfaces. Sci.

Total Environ. 427–428, 347–354. https://doi.org/10.1016/j.scitotenv.2012.03.084.
Sagnotti, L., Taddeucci, J., Winkler, A., Cavallo, A., 2009. Compositional, morphological, and hysteresis characterization of magnetic airborne particulate matter in Rome, Italy. Geochem. Geophys. Geosyst. 10 (8), n/a–n/a. https://doi.org/10.1029/2009GC002563.
Sagnotti, L., Winkler, A., 2012. On the magnetic characterization and quantification of the superparamagnetic fraction of traffic-related urban airborne PM in Rome, Italy. Atmos. Environ. 59, 131–140. https://doi.org/10.1016/j.atmosenv.2012.04.058.
Salvatori, E., Fusaro, L., Manes, F., 2016. Chlorophyll fluorescence for phenotyping drought-stressed trees in a mixed deciduous forest. Annali di Botanica 6, 39–49. https://doi.org/10.4462/annbotrm-13263.
Salvatori, E., Fusaro, L., Mereu, S., Bernardini, A., Puppi, G., Manes, F., 2013. Different O3 response of sensitive and resistant snap bean genotypes (*Phaseolus vulgaris* L.): the key role of growth stage, stomatal conductance, and PSI activity. Environ. Exp. Bot. 87, 79–91. https://doi.org/10.1016/j.envexpbot.2012.09.008.
di Toppi, S., Luigi, S., di Toppi, L., Bellini, E., 2020. Novel Coronavirus: how atmospheric particulate affects our environment and health. Challenges 11, 6. https://doi.org/10.3390/challe11010006.
Sebastiani, A., Marando, F., Manes, F., 2021. Mismatch of regulating ecosystem services for sustainable urban planning: PM10 removal and urban heat island effect mitigation in the municipality of Rome (Italy). Urban For. Urban Green. 57, 126938. https://doi.org/10.1016/j.ufug.2020.126938.
Setti, L., Passarini, F., De Gennaro, G., Barbieri, P., Perrone, M.G., Borelli, M., Palmisani, J., Di Gilio, A., Torboli, V., Fontana, F., Clemente, L., Pallavicini, A., Ruscio, M., Piscitelli, P., Miani, A., 2020. SARS-Cov-2RNA found on particulate matter of Bergamo in Northern Italy: first evidence. Environ. Res. 188, 109754. https://doi.org/10.1016/j.envres.2020.109754.
Sgrigna, G., Sæbø, A., Gawronski, S., Popek, R., Calfapietra, C., 2015. Particulate Matter deposition on Quercus ilex leaves in an industrial city of central Italy. Environ. Pollut. 197, 187–194. https://doi.org/10.1016/j.envpol.2014.11.030.
Simonetti, G., Conte, E., Perrino, C., Canepari, S., 2018. Oxidative potential of size-segregated PM in an urban and an industrial area of Italy. Atmos. Environ. 187, 292–300. https://doi.org/10.1016/j.atmosenv.2018.05.051.
Stevens, C.J., Bell, J.N.B., Brimblecombe, P., Clark, C.M., Dise, N.B., Fowler, D., Lovett, G.M., Wolseley, P.A., 2020. The impact of air pollution on terrestrial managed and natural vegetation. Philos. Trans. Royal Society A 378 (2183), 20190317. https://doi.org/10.1098/rsta.2019.0317.
Strasser, R.J., Tsimilli-Michael, M., Qiang, S., Goltsev, V., 2010. Simultaneous in vivo recording of prompt and delayed fluorescence and 820-nm reflection changes during drying and after rehydration of the resurrection plant Haberlea rhodopensis. Biochim. Biophys. Acta (BBA) 2010 1797, 1313–1326. https://doi.org/10.1016/j.bbabio.2010.03.008.
Szönyi, M., Sagnotti, L., Hirt, A.M., 2008. A refined biomonitoring study of airborne particulate matter pollution in Rome, with magnetic measurements on Quercus Ilex tree leaves. Geophys. J. Int. 173, 127–141. https://doi.org/10.1111/j.1365-246X.2008.03715.x.
Szönyi, M., Sagnotti, L., Hirt, A.M., 2007. On leaf magnetic homogeneity in particulate matter biomonitoring studies. Geophys. Res. Lett. 34 (6) https://doi.org/10.1029/2006GL029076.
Tung, N.T., Cheng, P.-C., Chi, K.-H., Hsiao, T.-C., Jones, T., BéruBé, K., Ho, K.-F., Chuang, H.-C., 2021. Particulate matter and SARS-CoV-2: a possible model of COVID-19 transmission. Sci. Total Environ. 750, 141532. https://doi.org/10.1016/j.scitotenv.2020.141532.
Valladares, F., Niinemets, Ü., 2008. Shade tolerance, a key plant feature of complex nature and consequences. Annu. Rev. Ecol. Evol. Syst. 39 (1), 237–257. https://doi.org/10.1146/annurev.ecolsys.39.110707.173506.
Violle, C., Navas, M.-L., Vile, D., Kazakou, E., Fortunel, C., Hummel, I., Garnier, E., 2007. Let the concept of trait be functional! Oikos 116, 882–892. https://doi.org/10.1111/j.0030-1299.2007.15559.x.
Winkler, A., Contardo, T., Vannini, A., Sorbo, S., Basile, A., Loppi, S., 2020. Magnetic emissions from brake wear are the major source of airborne particulate matter bioaccumulated by lichens exposed in Milan (Italy). Applied Sciences 10, 2073. https://doi.org/10.3390/app10062073.
World Health Organization, 2004. Health aspects of air pollution: results from the WHO project. Systematic review of health aspects of air pollution in Europe.
World Health Organization, 2014. 7 Million Premature Deaths Annu-ally Linked to Air Pollution (Article Online). Available from. http://www.who.int/mediacentre/news/releases/2014/air-pollution/en/.
Xu, X., Zhang, Z., Bao, L., Mo, L., Yu, X., Fan, D., Lun, X., 2017. Influence of rainfall duration and intensity on particulate matter removal from plant leaves. Sci. Total Environ. 609, 11–16. https://doi.org/10.1016/j.scitotenv.2017.07.141.
Yao, Y., Pan, J., Wang, W., Liu, Z., Kan, H., Qiu, Y., Meng, X., Wang, W., 2020. Association of particulate matter pollution and case fatality rate of COVID-19 in 49 Chinese cities. Sci. Total Environ. 741, 140396. https://doi.org/10.1016/j.scitotenv.2020.140396.
Zoran, M.A., Savastru, R.S., Savastru, D.M., Tautan, M.N., 2020. Assessing the relationship between surface levels of $PM_{2.5}$ and $PM_{10}$ particulate matter impact on COVID-19 in Milan, Italy. Sci. Total Environ. 738, 139825. https://doi.org/10.1016/j.scitotenv.2020.139825.